



CHORUS

This is the accepted manuscript made available via CHORUS. The article has been published as:

Anomalous electron transport in epitaxial NdNiO₃ films

Shashank Kumar Ojha, Sujay Ray, Tanmoy Das, S. Middey, Sagar Sarkar, Priya Mahadevan, Zhen Wang, Yimei Zhu, Xiaoran Liu, M. Kareev, and J. Chakhalian

Phys. Rev. B **99**, 235153 — Published 27 June 2019

DOI: [10.1103/PhysRevB.99.235153](https://doi.org/10.1103/PhysRevB.99.235153)

Anomalous electron transport in epitaxial NdNiO₃ films

Shashank Kumar Ojha, Sujay Ray, Tanmoy Das, and S. Middey*
Department of Physics, Indian Institute of Science, Bengaluru 560012, India

Sagar Sarkar and Priya Mahadevan
S.N. Bose National Center for Basic Sciences, JD-Block, Sector III, Salt Lake, Kolkata 700098, India

Zhen Wang and Yimei Zhu
*Department of Condensed Matter Physics and Materials Science,
Brookhaven National Laboratory, Upton, NY, 11973, USA*

Xiaoran Liu, M. Kareev, and J. Chakhalian
Department of Physics and Astronomy, Rutgers University, Piscataway, New Jersey 08854, USA

The origin of simultaneous electronic, structural and magnetic transitions in bulk rare-earth nickelates ($RENiO_3$) remains puzzling with multiple conflicting reports on the nature of these entangled phase transitions. Heterostructure engineering of these materials offers unique opportunity to decouple metal-insulator transition (MIT) from the magnetic transition. However, the evolution of underlying electronic properties across these decoupled transitions remains largely unexplored. In order to address this, we have measured Hall effect on a series of epitaxial NdNiO₃ films, spanning a variety of electronic and magnetic phases. We find that the MIT results in only partially gapped Fermi surface, whereas full insulating phase forms below the magnetic transition. In addition, we also find a systematic reduction of the Hall coefficient (R_H) in the metallic phase of these films with epitaxial strain and also a surprising transition to negative value at large compressive strain. Partially gapped weakly insulating, paramagnetic phase is reminiscent of pseudogap behavior of high T_c cuprates. The precursor metallic phase, which undergoes transition to insulating phase is a non-Fermi liquid with the temperature exponent (n) of resistivity of 1, whereas the exponent increases to $4/3$ in the non-insulating samples. Such nickelate phase diagram with sign-reversal of R_H , pseudo-gap phase and non Fermi liquid behavior are intriguingly similar to high T_c cuprates, giving important guideline to engineer unconventional superconductivity in oxide heterostructure.

I. INTRODUCTION

The question about the nature of metal-insulator transition (MIT) and spin ordering in the negative charge transfer family of materials $RENiO_3$ ($RE=Pr, Nd...Lu$ etc.) has drawn a significant interest in the pursuit of understanding the ultimate connection among the underlying crystal structure, electronic, and magnetic orderings¹⁻²³. Independently, there has been a number of interesting theoretical proposals to realize high temperature superconductivity through epitaxial engineering²⁴⁻²⁸, leading to the remarkable progress in synthesis and characterization of ultra-thin film and heterostructures of rare-earth nickelates (for recent progress see Refs. 3 and 4 for review and the references therein). Since the degeneracy lifting between two e_g orbitals of Ni^{3+} ions might lead to cuprate-like one band Fermi surface, orbital engineering of $RENiO_3$ have been also attempted in various heterostructure forms^{3,29-34}. However, to-date maximum achieved orbital polarization of nickelate heterostructures ($\sim 25\%$) is still significantly smaller than that which is required to architecture the materials analog of high T_c cuprates. Therefore, it is of a paramount interest to find out if and how epitaxy can be utilized to finally achieve cuprate like electronic structure in $RENiO_3$ based heterostructures.

Hall effect is an important measurement which provides crucial information about the Fermi surface topology, the carrier concentration, the anisotropy of scattering rate, and the chiral spin textures of quantum materials³⁵⁻³⁸. In connec-

tion to nickelates, earlier studies on bulk NdNiO₃ (NNO) and PrNiO₃ (PNO) powder samples demonstrated the phenomenon of sign change of Hall coefficient (R_H) across the metal-insulator transition³⁹. Interestingly, such evolution of R_H has been also observed in several important ‘bad’ metals including cuprates, vanadates, and ruthenates; this phenomenon was attributed to multiple factors including structural transition, spin density wave (SDW) transition, charge density wave (CDW) transition⁴⁰⁻⁴³. Therefore, the simultaneous occurrence of MIT, structural transition, charge (CO) and magnetic ordering in bulk NNO and PNO^{6,44-46} inhibits the straightforward determination of the primary factor responsible for such drastic change in R_H . On the other hand, these simultaneous transitions can be selectively decoupled or even suppressed by epitaxial strain in ultra-thin film geometry^{12,13,15,47-49}. Naturally, in such situation one can expect that the Hall effect measurement will provide crucial information about the electronic and magnetic transitions. Further, it is interesting to note that epitaxial strain dramatically affects the electronic properties in the metallic phase of nickelate films as highlighted by the change in the characteristic power-exponents of resistivity, associated with the non-Fermi liquid behavior^{47,48,50}. This observation suggests that Hall effect measurements in the metallic phase can probe the relative change in Fermi surface topology brought about by epitaxial strain⁵¹.

In this paper, we report on the detailed Hall effect measurements across several electronic and magnetic phases of

NNO, which have been realized in a series of epitaxially stabilized high-quality ultra-thin films on several single crystalline substrates. These measurements have revealed a direct link between the sign change of R_H and the onset of E' antiferromagnetic (E' -AFM⁴⁶) transition implying a SDW (spin density wave) origin of the puzzling E' -AFM phase. Such magnetic transition driven by the Fermi surface reconstruction has been predicted by earlier theoretical works^{7,8}. Moreover, metallic phase of the NNO film under large tensile strain exhibits unexpected cuprate-like linearly T -dependent resistivity and T^2 dependence of cotangent of Hall angle. The magnitude of R_H in the metallic phase shows a systematic decrease with the underlying strain and remains positive down to lowest temperatures under moderate compressive strain. Upon application of large compressive strain, surprisingly negative R_H ($T > 60$ K) emerges in the metallic phase, emphasizing a drastic change in Fermi surface topology. The decrease (increase) in hole (electron) concentration without any chemical doping illustrates a strain mediated self-doping scenario, which is further verified by density functional theory (DFT). Our further analysis using DFT+MRDF (momentum resolved density fluctuation) method found that the suppression of E' -AFM ordering by epitaxial strain can be accounted by the suppression of Fermi surface nesting.

II. METHODS

Ultra-thin films of NNO (15 unit cell=u.c.) of high structural and chemical quality have been grown on several single crystalline substrates [see Fig. 1(a)]: SrTiO₃ (STO), NdGaO₃ (NGO), SrPrGaO₄ (SPGO), SrLaAlO₄ (SLAO) and YAlO₃ (YAO). The details of the growth procedure can be found in Ref. 47. The in-plane pseudocubic lattice constants of all used substrates and the corresponding strain (ϵ) values are summarized in Fig. 1(b). The layer-by-layer growth has been monitored by in-situ RHEED (see supplemental⁵²) and the desired epitaxial growth along a pseudo-cubic [0 0 1] direction has

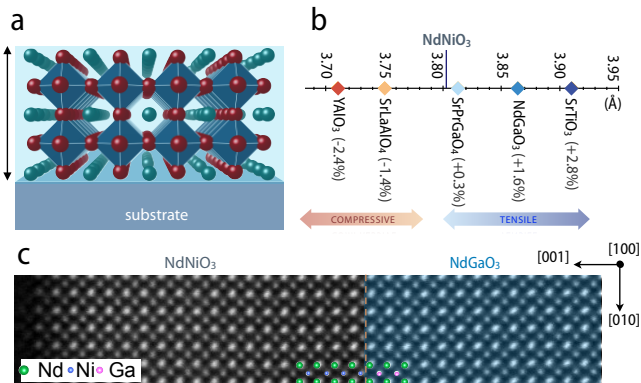


FIG. 1. (a) NdNiO₃ thin film on single crystalline substrate. (b) Pseudocubic in-plane lattice constant for the substrates used in this work and the corresponding epitaxial strain for NNO. (c) HAADF-STEM image (with false color) of a 20 u.c. NdNiO₃ film on NdGaO₃ substrate.

been confirmed by X-ray diffraction⁵². A sample for cross-section STEM (scanning transmission electron microscopy) measurement has been prepared by a focused ion beam with Ga⁺ ions followed by Ar⁺ ions nano-milling. High-angle annular dark-field (HAADF) imaging has been achieved with a JEOL ARM200 microscope equipped with two aberration correctors. Figure 1(c) shows a characteristic HAADF-STEM image taken across the NNO/NGO interface along [1 0 0] direction; The atomic column intensity in the HAADF-STEM imaging varies with the atomic number as $\propto Z^{1.7}$, i.e. heavier atoms indicate brighter columns. As marked by the dashed line, the NGO substrate terminates with the NdO layer with practically atomically sharp interface which further testifies for the excellent registry between the sample and substrate. *dc* resistivity and Hall effect measurements have been carried out in four-probe van der Pauw geometry using a Quantum Design PPMS (Physical Property Measurement System). For evaluating R_H magnetic field (H) has been swept between ± 5 T at different T . In the absence of anomalous Hall contribution, while the intrinsic Hall resistance (R_{xy}) should be zero at $H = 0$ and asymmetric with magnetic field sweep, the finite width of contacts adds an additional symmetric part in R_{xy} about $H = 0$ with a vertical offset^{53,54}. These parasitic contributions were corrected to extract intrinsic R_{xy} and three typical sets of such corrected R_{xy} curves as a function of H for different T are presented in the Supplemental⁵². As clearly seen, after correction R_{xy} remains linear within the ranges of magnetic field (H) used in this work; Hall coefficient has been evaluated as $R_H = t(dR_{xy}/dH)$ where t is the film thickness.

To gain further insight of the change in R_H in the metallic phase of the samples as a function of epitaxial strain, we have performed density functional theory (DFT) calculation using the Vienna *ab-initio* simulation package^{55,56} within the GGA+ U of PBE parametrization⁵⁷. Projected augmented-wave (PAW)^{58,59} pseudo-potentials were used to describe core electrons. We use $U = 3.5$ eV, which is larger than the values of U used in the self-energy calculation. This is expected since the bare U used in the self-energy calculation is further multiplied by various components of the susceptibility to provide the effective many-body potential in this calculation as detailed below. The electronic wave-function is expanded using plane waves up to a cutoff energy of 500 eV. Brillouin zone (BZ) sampling is done by using a $(12 \times 12 \times 6)$ Monkhorst-Pack k -grid. Similar to Ref. 47, NdNiO₃ crystal structures have been constrained to $P4/mmm$ space group in our calculation and A type antiferromagnetic spin ordering on Ni sublattice has been imposed, instead of complex E' -AFM spin configuration. Octahedral tilts/rotations and breathing mode distortions have been also omitted in our calculations and the effect of substrates have been folded in to the experimental lattice constants. Despite these constraints, such DFT approach was shown to successfully reproduce the experimentally observed band structure and Fermi surface topology of NNO thin films on different substrates⁶⁰. The effects of electronic correlations on the band structure have been investigated by DFT and DFT+self energy corrections, obtained by MRDF theory (details of this calculation are in Supplemental Information)⁶⁰⁻⁶³.

TABLE I. Metal-insulator transition temperature (T_{MIT}) and antiferromagnetic ordering temperature (T_N), evaluated from ρ_{xx} vs. T data. c and h correspond to cooling and heating cycle, respectively.

Film	T_{MIT}^c	T_{MIT}^h	T_N^c	T_N^h
NdNiO ₃ on SrTiO ₃	145 K	155 K	90±5 K	110±5 K
NdNiO ₃ on NdGaO ₃	170 K	175 K	140 K	155 K

III. RESULTS AND DISCUSSIONS

A. Hall coefficient across electronic and magnetic transitions

The upper panels of Fig. 2(a)-(c) show the temperature dependent resistivity of NNO films under tensile strain. As reported earlier^{47,48}, NNO films under tensile strain show the first order MIT. Metal-insulator transition temperature T_{MIT} [defined as the temperature where $d\rho_{xx}/dT=0$] and magnetic transition temperature T_N [evaluated from $d(\ln\rho_{xx})/d(1/T)$ vs. T plot (right axis of lower panel of Fig. 2(a)-(b))⁶⁴] of these films are listed in Table-I. Note, lower value of T_{MIT} compared to the bulk NNO $T_{MIT} = T_N \sim 200$ K were linked to the effect of epitaxial strain (bandwidth control) and reduced dimensionality (quantum confinement)⁴⁷. Moreover, previous reports using resonant X-ray scattering (RXS) on such NNO films have confirmed the absence of both bulk-like charge ordering and lattice symmetry change across the MIT^{13,15}. Separation between T_{MIT} and T_N of these samples offers a unique temperature window to examine the evolution of R_H across all three phases: paramagnetic metal (PM), paramagnetic insulator (PI) and antiferromagnetic insulator (AFI) without influence of charge disproportionation (CD) and structural transition. While a bulk-like MIT and magnetic transition is expected in epitaxial NNO film under very small tensile strain of +0.3%, surprisingly the film shows only weakly insulating, paramagnetic behavior at low temperature⁴⁷ [see upper panel in Fig. 2(c)].

In the following, we discuss overall response of R_H across the electronic and magnetic transitions of these films. The temperature dependence of ρ_{xx} and R_H in the metallic phase will be presented latter in the text. As immediately seen in Fig. 2(a)-(c) at room temperature R_H is hole-like. Though the electronic structure of the system is expected to be drastically different across the metal-insulator transition, R_H exhibits only a slight increase across T_{MIT} for the NNO film on NGO and STO. Most interestingly, R_H switches to n-type around 100 K and 120 K for STO and NGO cases respectively, which are remarkably close to the respective T_N for E' -AFM ordering. Similar sign change of R_H across T_N has been also observed in 2EuNiO₃/1LaNiO₃ superlattice, which has monoclinic symmetry in both metallic and insulating phase and does not exhibit any charge ordering transition²¹. R_H maintains hole-like behavior even in the weakly insulating state for the film grown on SPGO substrate, where earlier RXS experiments⁴⁷ had clearly ruled out the appearance of E' -type magnetic ordering. All of these observations clearly point at some large changes in the Fermi surface topology to be responsible for the appearance for E' -type antiferromagnetic ordering in

these materials.

The mechanisms of the MIT and E' type AFM ordering of $RENiO_3$ is still heavily debated^{5-18,20-23}. Most recently, the MIT mechanism has been attributed to the $d^8\bar{L}+d^8\bar{L} \rightarrow d^8+d^8\bar{L}^2$ bond disproportionation (BD) transition (here \bar{L} denotes a ligand hole in O p bands)^{5,10,11,14,17,21,65}. Apart from the BD induced transition scenario, the importance of Mott physics in realization of the insulating phase has been found in optical conductivity measurements^{9,65}. Another unexpected result was revealed in the recent valence band photoemission measurement which showed the presence of residual intensity at E_F even in very low T thus signalling that some parts of the Fermi surface still survive deep into the insulating phase⁶⁶. Such notion of a partially gapped Fermi surface, akin to the pseudogap phase of high T_c cuprate, ruthenates, pnictides etc.⁶⁷⁻⁶⁹ was also inferred for NNO from IR spectroscopy⁹ and tunneling spectroscopy measurement⁷⁰.

Since R_H is magnetic field independent within the range of magnetic field used in this present study it can be expressed as $R_H = (n_p\mu_p^2 - n_e\mu_e^2)/e(n_p\mu_p + n_e\mu_e)^2$, assuming one electron band and one hole band are contributing to the electrical transport, where n_p (n_e) is the hole (electron) density and μ_p (μ_e) is the mobility of the hole (electron)⁷¹. The positive sign of R_H in the paramagnetic metallic phases^{49,54,72} originates from the larger volume of the hole pockets (v_p) compared to the electron pockets (v_e) as observed in ARPES experiments^{60,73}. Small increase of R_H upon entering into the insulating phase suggests that the BD transition opens only a partial gap in Fermi surface. ARPES measurement⁷³ found a strong instability at $\mathbf{q} = (1/4, 1/4, 1/4)_{p.c.}$, which also coincides with the magnetic wave-vector for E' ordering. Thus the nesting of dominant hole pockets in BD phase opens gap in the hole Fermi surface and results in the emergence of E' -AFM phase^{7,8,12,49,54,74} with the remaining electron pockets contributing to the transport to result the observed switching of R_H across T_N . Once BD phase and E' -AFM ordering set in, they act synergetically to grow together with the decrease of thermal fluctuations⁷⁵. Complimentary experiments, like ARPES measurements at different T are required to fully understand the evolution of R_H with T in AFI phase. On lowering of tensile strain, the suppression of the Fermi surface superstructure at $(1/4, 1/4, 1/4)_{p.c.}$ is found to be responsible for the absence of E' -AFM phase in NNO film on SPGO substrate where R_H remains positive in such paramagnetic BD phase (results are shown in the Supplemental⁵²).

B. ρ_{xx} and R_H in metallic phase

Next we explore magneto-transport behavior in the metallic phase. Contrary to the expected T^2 dependence of resistivity at low temperature for a Fermi liquid, ρ_{xx} in the metallic phases of NNO under tensile strain show *linear* T dependent behavior (see Supplemental⁵²). As reported earlier⁴⁷, the electronic and magnetic transitions can be entirely suppressed by the application of compressive strain [see Fig. 3(a)]. Interestingly, under compressive strain ρ_{xx} shows $T^{4/3}$ dependence over a broad range of temperatures and then switches to linear

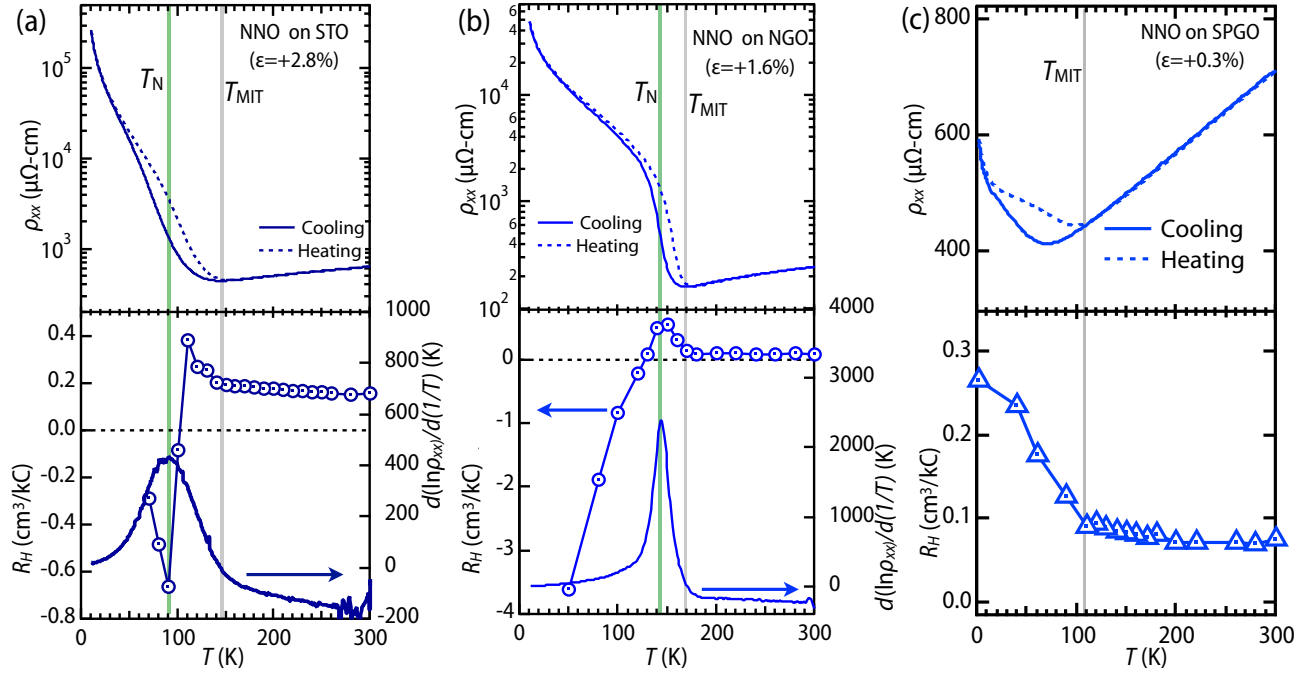


FIG. 2. Temperature dependence of dc resistivity of 15 u.c. NNO film under tensile strain in upper panel of (a)-(c). The variation of R_H are shown in corresponding lower panel. Right axis of the lower panel of (a) and (b) corresponds to $d(\ln\rho_{xx})/d(1/T)$ vs. T plot.

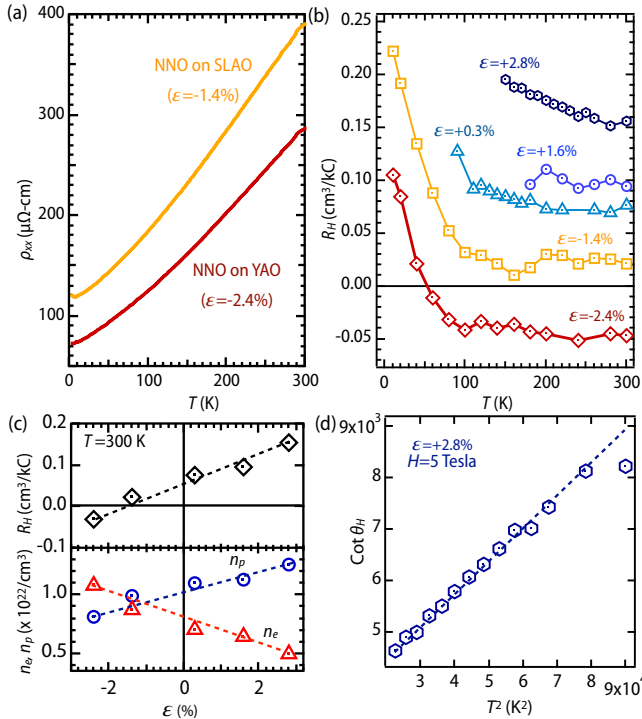


FIG. 3. (a) Temperature dependence of dc resistivity for 15 u.c. NNO film under compressive strain. (b) Temperature dependence of R_H in the paramagnetic metallic phase of the NNO films. (c) Relation of R_H (upper panel), carrier density (lower panel) with strain at 300 K. (d) $\cot\theta_H$ for the NNO film on STO substrate as a function of T^2 . The dotted line represents T^2 dependence.

T behavior⁵². Such non Fermi liquid behavior has been observed in the normal phase of several unconventional superconductors including cuprates, organic superconductor, pnictides, heavy-fermions etc.⁷⁶⁻⁷⁹ and its intrinsic origin is still unknown^{80,81}.

The overall behavior of R_H in the metallic phase is summarized in Fig. 3(b). As seen, the NNO film grown on SLAO substrate (-1.2%) exhibits a p -type metallic behavior over the entire temperature range. With the further increase of compressive strain (NNO on YAO), R_H surprisingly becomes negative even at 300 K. A systematic relation between $R_H|_{T=300\text{K}}$ and ϵ can be further inferred from the upper panel of Fig. 3(c). Such strain mediated change in carrier density shown in Fig. 3(c) is a hallmark of the self-doping effect⁵².

For a normal metal, R_H generally becomes temperature independent for $T > 0.2-0.4 \Theta_D$ (Θ_D is Debye temperature)⁸². Since for $RENiO_3$ $\Theta_D \sim 420$ K⁸³, strong T dependent R_H in the metallic phase of NNO film on STO requires some special consideration. For this purpose we recap that in hole doped cuprates the strong T dependence of R_H is commonly discussed in terms of the Hall angle $\cot\theta_H = \rho_{xx}/(HR_H)$. The T^2 dependence of the $\cot\theta_H$, observed in hole-doped cuprates around optimal doping has been interpreted as a signature of spin-charge separation or result of anisotropic scattering rates^{82,84-87}. However, R_H becomes T -independent in lightly hole doped cuprates and consequently $\cot\theta_H$ follows the T dependence of ρ_{ab} ³⁶. Based on these results, we can speculate that T^2 dependence of $\cot\theta_H$ [Fig. 3(c)] and linear T dependence of ρ_{xx} for the NNO film on STO implies a strong connection with the 'strange metal' phase of high T_c cuprates. As shown in Fig. 3(b), with the decrease of hole concentra-

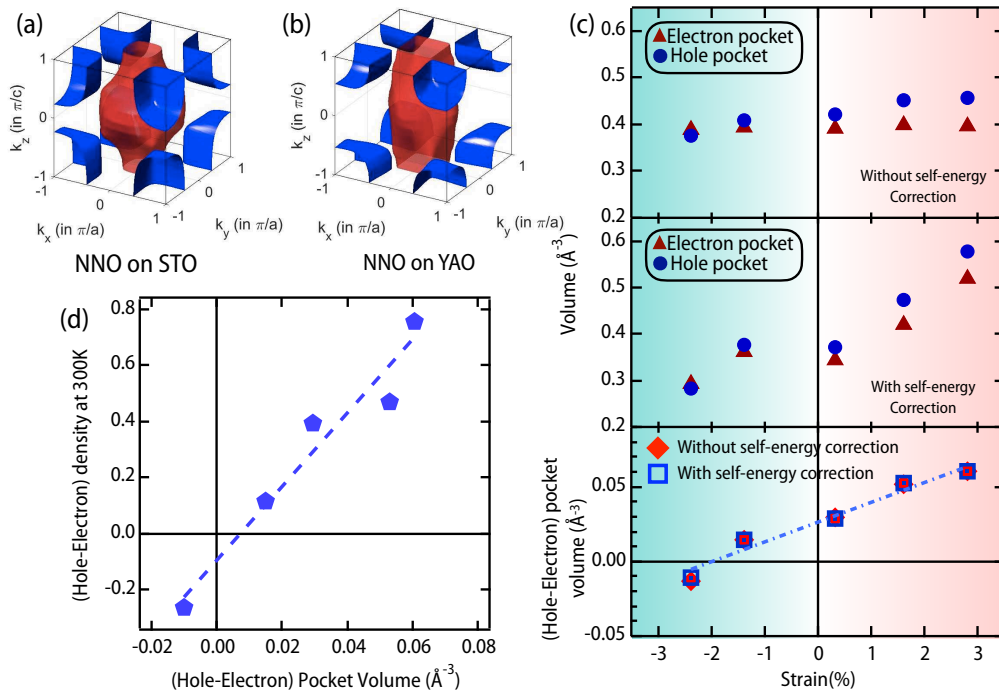


FIG. 4. (a)-(b) Computed FS topology are shown for the two representative samples of NNO/STO and NNO/YAO. a in x and y axes of these graphs correspond to in-plane pseudo cubic lattice constant of the substrate. For z axis, $c \sim 2c_{p.c.}$, where $c_{p.c.}$ is out-of plane lattice constant of NNO film. Details of Brillouin zone have been discussed in Supplemental information⁵². (c) FS volume for electron (triangle) and hole (circles) pockets are compared for all samples without (top panel) and with (middle) self-energy corrections. Bottom panel compares the difference between the hole and electron pocket volume for calculations without (filled diamond) and with (open square) self-energy effects. (d) Comparison of the difference between the two FS volume with the experimental value of the effective carrier density obtained from Hall effect.

tion, R_H becomes almost T independent in the metallic phase of NNO film on NGO and at high temperatures for other compressive substrates. Such sharp increase in R_H below 100 K in compressively strained NNO can be attributed to the emergence of the pseudogap phase^{70,88}, which is observed in many cuprates and yet a poorly understood phenomena^{36,85,89-91}. In addition, the sign change of R_H in pseudogap phase suggests that there is coexistence of electron and hole Fermi surface pockets with different mobility, as also seen in electron and hole doped cuprates^{40,92-94}. Our result further implies that the hole pocket has higher mobility compared to electron-pocket, which is consistent with prior ARPES data⁷³.

C. DFT calculation

In order to gain insight into the strain induced modulation of R_H in the metallic phase shown in Fig. 3(c), we have calculated Fermi surface (FS) of NNO for different values of ϵ , listed in Fig. 1(b). In all cases, we obtain a characteristic FS topology which consists of the electron-pocket at the center of the BZ and hole pockets at the zone corners. The computed FSs shown in Figs. 4(a) and 4(b) for large tensile (STO) and large compressive (YAO) strain exhibit the characteristic reduction of the 3-dimensionality electron pocket (electron

pocket is almost cylindrical for NNO on YAO) as a function of strain. In Figure 4(c), we summarize the evolution of FS volumes for the two pockets. As seen, despite the gradual loss of three-dimensionality in Fermi surface between NNO under +2.8% vs. NNO under -2.4%, the electron pocket volume remains essentially unchanged. On the other hand, the hole pocket volume is larger than electron pocket volume for all cases except for NNO on YAO. This is the key mechanism for the sign change in the Hall coefficient at high temperatures where paramagnetic metallic state appears in all samples.

Since Mott physics is clearly important in driving antiferromagnetic and insulating phases of nickelates^{9,22}, we have further tested the above DFT results with the inclusion of the self-energy correction due to electron-electron correlations. We compute the complex self-energy effects due to density-density fluctuations within the DFT+ MRDF theory⁶⁰⁻⁶³. The MRDF method directly incorporates the materials-specific DFT band structure and solve the Hubbard model (with intra and inter band Hubbard interactions) for the electron-electron correlation part; The electron correlations which arise due to spin and charge density fluctuations are computed within the random-phase approximation. The feedback effects of the correlation to the electronic spectrum is captured within the fluctuation-exchange (FLEX) method and quantified by band (ν), momentum (\mathbf{k}) and frequency (ω) dependent complex

self-energy $\Sigma_\nu(\mathbf{k}, \omega)$ corrections. We invoke self-consistency in such a way that the spin and charge correlation functions and the electronic Green's function include the self-energy corrections until the convergence in the self-energy value is reached⁵².

The interacting Fermi surface is defined by the poles of the interacting Green's function at $\omega = 0$ which is obtained from the self-consistent solution of $\varepsilon'_{\mathbf{k}_F} + \Sigma'_\nu(\mathbf{k}_F, \omega = 0) = 0$ where $\varepsilon'_{\mathbf{k}}$ denotes the ν^{th} DFT band at momentum \mathbf{k} and Σ'_ν represent the real parts of the self-energy. We note that since self-energy is momentum dependent, the above solution can lead to a band-dependent change in shape of the Fermi surface. In what follows the \mathbf{k} -dependent self-energy causes a non-rigid-band shift of the Fermi surface, yet the total Fermi surface area remaining unchanged. This FS volume calculated with the self-energy dressed bands is shown in Fig. 4(c) middle panel). As seen, we obtain a non-monotonic behavior of the FS volume across different samples. However, in all cases, we find a one-to-one correspondence to the non-interacting FS volume, in that the electron pocket area is lower than that of the hole -pocket one, except for NNO on YAO. Thus, strain induced n -type metallic phase of NNO film results from the change in relative FS volume by compressive epitaxy.

To further testify that the estimated effective FS volume (δv_{FS}) truly correspond to the experimentally observed switching in R_H as a function of ϵ , we plot δv_{FS} as a function of the difference in carrier concentration, $\delta n = n_p - n_e$ (n_p, n_e have been estimated from experimentally found R_H at 300 K). The linear relation between δv_{FS} and δn shown in Fig. 4(d) clearly testifies for the validity of our approach to capture the experimental observations.

IV. CONCLUSIONS

To summarize, we have synthesized and measured Hall effect on a series of ultra-thin NdNiO₃ films. The selective

suppression of the simultaneous transitions in NdNiO₃ films through epitaxial strain engineering enable us to probe the paramagnetic metallic, paramagnetic insulating and antiferromagnetic insulating phases separately, without any detrimental influence of structural and charge ordering transitions. This approach reveals an unusual sign change in Hall coefficient across the E' -type antiferromagnetic transition. The appearance of such spin density wave transition from a paramagnetic insulating phase signals that the bond-disproportionation transition creates a partially gapped Fermi surface. Epitaxial strain also drastically changes the relative volume between hole and electron parts of the Fermi surface, resulting in a strain driven sign change in R_H in the metallic phase of NNO. Under compressive strain, all of the NNO films exhibit a non-Fermi liquid (NFL) behavior with algebraic power exponents whereas the film under large tensile strain shows magneto-transport behavior akin to the 'strange metal' phase of optimally doped high T_c cuprates. While superconductivity remains elusive in the nickelate heterostructures so far, these systems host several remarkable high T_c cuprate signatures including Zhang-Rice state, pseudogap, self-doping, NFL behavior with linear T resistivity, and spin-density wave.

V. ACKNOWLEDGEMENT

SM acknowledges IISc start up grant, DST Nanomission (grant No. DST/NM/NS/2018/246), and SERB Early Career Research Award (ECR/2018/001512) for the financial support. J.C. is funded by Gordon and Betty Moore Foundation EPiQS Initiative through Grant GBMF4534. This research used resources of the Center for Functional Nanomaterials, which is a U.S. DOE Office of Science Facility, at Brookhaven National Laboratory under Contract No. DE-SC0012704

* smiddey@iisc.ac.in

¹ M. L. Medarde, Journal of Physics: Condensed Matter **9**, 1679 (1997).
² G. Catalan, *Phase Transitions* **81**, 729 (2008).
³ S. Middey, J. Chakhalian, P. Mahadevan, J. W. Freeland, A. J. Millis, and D. D. Sarma, *Annual Review of Materials Research* **46**, 305 (2016).
⁴ S. Catalano, M. Gibert, J. Fowlie, J. Íñiguez, J.-M. Triscone, and J. Kreisel, *Reports on Progress in Physics* **81**, 046501 (2018).
⁵ T. Mizokawa, D. I. Khomskii, and G. A. Sawatzky, *Phys. Rev. B* **61**, 11263 (2000).
⁶ U. Staub, G. I. Meijer, F. Fauth, R. Allenspach, J. G. Bednorz, J. Karpinski, S. M. Kazakov, L. Paolasini, and F. d'Acapito, *Phys. Rev. Lett.* **88**, 126402 (2002).
⁷ S. Lee, R. Chen, and L. Balents, *Phys. Rev. Lett.* **106**, 016405 (2011).
⁸ S. Lee, R. Chen, and L. Balents, *Phys. Rev. B* **84**, 165119 (2011).
⁹ M. K. Stewart, J. Liu, M. Kareev, J. Chakhalian, and D. N. Basov, *Phys. Rev. Lett.* **107**, 176401 (2011).

¹⁰ H. Park, A. J. Millis, and C. A. Marianetti, *Phys. Rev. Lett.* **109**, 156402 (2012).
¹¹ S. Johnston, A. Mukherjee, I. Elfimov, M. Berciu, and G. A. Sawatzky, *Phys. Rev. Lett.* **112**, 106404 (2014).
¹² M. Hepting, M. Minola, A. Frano, G. Cristiani, G. Logvenov, E. Schierle, M. Wu, M. Bluschke, E. Weschke, H.-U. Habermeier, E. Benckiser, M. Le Tacon, and B. Keimer, *Phys. Rev. Lett.* **113**, 227206 (2014).
¹³ M. H. Upton, Y. Choi, H. Park, J. Liu, D. Meyers, J. Chakhalian, S. Middey, J.-W. Kim, and P. J. Ryan, *Phys. Rev. Lett.* **115**, 036401 (2015).
¹⁴ A. Subedi, O. E. Peil, and A. Georges, *Phys. Rev. B* **91**, 075128 (2015).
¹⁵ D. Meyers, J. Liu, J. W. Freeland, S. Middey, M. Kareev, J. Kwon, J. M. Zuo, Y.-D. Chuang, J. W. Kim, P. J. Ryan, and et al., *Scientific Reports* **6**, 27934 (2016).
¹⁶ R. J. Green, M. W. Haverkort, and G. A. Sawatzky, *Phys. Rev. B* **94**, 195127 (2016).

- ¹⁷ V. Bisogni, S. Catalano, R. J. Green, M. Gibert, R. Scherwitzl, Y. Huang, V. N. Strocov, P. Zubko, S. Balandeh, J.-M. Triscone, and et al., *Nature Communications* **7**, 13017 (2016).
- ¹⁸ K. Haule and G. L. Pascut, *Scientific Reports* **7**, 2045 (2017).
- ¹⁹ B. Mandal, S. Sarkar, S. K. Pandey, P. Mahadevan, C. Franchini, A. J. Millis, and D. D. Sarma, (2017), [arXiv:1701.06819](https://arxiv.org/abs/1701.06819).
- ²⁰ Y. Lu, D. Betto, K. Fürsich, H. Suzuki, H.-H. Kim, G. Cristiani, G. Logvenov, N. B. Brookes, E. Benckiser, M. W. Haverkort, G. Khaliullin, M. Le Tacon, M. Minola, and B. Keimer, *Phys. Rev. X* **8**, 031014 (2018).
- ²¹ S. Middey, D. Meyers, M. Kareev, Y. Cao, X. Liu, P. Shafer, J. W. Freeland, J.-W. Kim, P. J. Ryan, and J. Chakhalian, *Phys. Rev. Lett.* **120**, 156801 (2018).
- ²² A. Mercy, J. Bieder, J. Íñiguez, and P. Ghosez, *Nature Communications* **8**, 1677 (2017).
- ²³ J. Shamblin, M. Heres, H. Zhou, J. Sangoro, M. Lang, J. Neuefeind, J. A. Alonso, and S. Johnston, *Nature Communications* **9**, 86 (2018).
- ²⁴ J. c. v. Chaloupka and G. Khaliullin, *Phys. Rev. Lett.* **100**, 016404 (2008).
- ²⁵ P. Hansmann, X. Yang, A. Toschi, G. Khaliullin, O. K. Andersen, and K. Held, *Phys. Rev. Lett.* **103**, 016401 (2009).
- ²⁶ P. Hansmann, A. Toschi, X. Yang, O. K. Andersen, and K. Held, *Phys. Rev. B* **82**, 235123 (2010).
- ²⁷ M. J. Han, X. Wang, C. A. Marianetti, and A. J. Millis, *Phys. Rev. Lett.* **107**, 206804 (2011).
- ²⁸ M. J. Han, X. Wang, C. A. Marianetti, and A. J. Millis, *Phys. Rev. Lett.* **110**, 179904 (2013).
- ²⁹ E. Benckiser, M. W. Haverkort, S. Brück, E. Goering, S. Macke, A. Fraaije, X. Yang, O. K. Andersen, G. Cristiani, H.-U. Habermeier, A. V. Boris, I. Zegkinoglou, P. Wochner, H.-J. Kim, V. Hinkov, and B. Keimer, *Nat Mater* **10**, 189 (2011).
- ³⁰ J. W. Freeland, J. Liu, M. Kareev, B. Gray, J. W. Kim, P. J. Ryan, R. Pentcheva, and J. Chakhalian, *Europhysics Letters* **96**, 57004 (2011).
- ³¹ J. Chakhalian, J. M. Rondinelli, J. Liu, B. A. Gray, M. Kareev, E. J. Moon, N. Prasai, J. L. Cohn, M. Varela, I. C. Tung, M. J. Bedzyk, S. G. Altendorf, F. Strigari, B. Dabrowski, L. H. Tjeng, P. J. Ryan, and J. W. Freeland, *Phys. Rev. Lett.* **107**, 116805 (2011).
- ³² M. Wu, E. Benckiser, M. W. Haverkort, A. Frano, Y. Lu, U. Nwankwo, S. Brück, P. Audehm, E. Goering, S. Macke, V. Hinkov, P. Wochner, G. Christiani, S. Heinze, G. Logvenov, H.-U. Habermeier, and B. Keimer, *Phys. Rev. B* **88**, 125124 (2013).
- ³³ A. S. Disa, F. J. Walker, S. Ismail-Beigi, and C. H. Ahn, *APL Materials* **3**, 062303 (2015).
- ³⁴ S. Middey, D. Meyers, D. Doennig, M. Kareev, X. Liu, Y. Cao, Z. Yang, J. Shi, L. Gu, P. J. Ryan, R. Pentcheva, J. W. Freeland, and J. Chakhalian, *Phys. Rev. Lett.* **116**, 056801 (2016).
- ³⁵ N. P. Ong and P. W. Anderson, *Phys. Rev. Lett.* **78**, 977 (1997).
- ³⁶ Y. Ando, Y. Kurita, S. Komiya, S. Ono, and K. Segawa, *Phys. Rev. Lett.* **92**, 197001 (2004).
- ³⁷ S. Ono, S. Komiya, and Y. Ando, *Phys. Rev. B* **75**, 024515 (2007).
- ³⁸ N. Nagaosa and Y. Tokura, *Nature Nanotechnology* **8**, 899 (2013).
- ³⁹ S.-W. Cheong, H. Hwang, B. Batlogg, A. Cooper, and P. Canfield, *Physica B: Condensed Matter* **194-196**, 1087 (1994).
- ⁴⁰ D. LeBoeuf, N. Doiron-Leyraud, J. Levallois, R. Daou, J.-B. Bonnemaison, N. Hussey, L. Balicas, B. Ramshaw, R. Liang, D. Bonn, et al., *Nature* **450**, 533 (2007).
- ⁴¹ H.-T. Kim, Y. W. Lee, B.-J. Kim, B.-G. Chae, S. J. Yun, K.-Y. Kang, K.-J. Han, K.-J. Yee, and Y.-S. Lim, *Phys. Rev. Lett.* **97**, 266401 (2006).
- ⁴² L. M. Galvin, R. S. Perry, A. W. Tyler, A. P. Mackenzie, S. Nakatsuji, and Y. Maeno, *Phys. Rev. B* **63**, 161102 (2001).
- ⁴³ H. Xing, L. Wen, C. Shen, J. He, X. Cai, J. Peng, S. Wang, M. Tian, Z.-A. Xu, W. Ku, Z. Mao, and Y. Liu, *Phys. Rev. B* **97**, 041113 (2018).
- ⁴⁴ J. E. Lorenzo, J. L. Hodeau, L. Paolasini, S. Lefloch, J. A. Alonso, and G. Demazeau, *Phys. Rev. B* **71**, 045128 (2005).
- ⁴⁵ V. Scagnoli, U. Staub, M. Janousch, A. M. Mulders, M. Shi, G. I. Meijer, S. Rosenkranz, S. B. Wilkins, L. Paolasini, J. Karpinski, S. M. Kazakov, and S. W. Lovesey, *Phys. Rev. B* **72**, 155111 (2005).
- ⁴⁶ V. Scagnoli, U. Staub, A. M. Mulders, M. Janousch, G. I. Meijer, G. Hammerl, J. M. Tonnerre, and N. Stojic, *Phys. Rev. B* **73**, 100409 (2006).
- ⁴⁷ J. Liu, M. Kargarian, M. Kareev, B. Gray, P. J. Ryan, A. Cruz, N. Tahir, Y.-D. Chuang, J. Guo, J. M. Rondinelli, J. W. Freeland, G. A. Fiete, and J. Chakhalian, *Nat Commun* **4**, 2714 (2013).
- ⁴⁸ E. Mikheev, A. J. Hauser, B. Himmetoglu, N. E. Moreno, A. Janotti, C. G. Van de Walle, and S. Stemmer, *Science Advances* **1**, e1500797 (2015), <http://advances.sciencemag.org/content/1/10/e1500797.full.pdf>.
- ⁴⁹ A. J. Hauser, E. Mikheev, N. E. Moreno, J. Hwang, J. Y. Zhang, and S. Stemmer, *Applied Physics Letters* **106**, 092104 (2015).
- ⁵⁰ S. Middey, D. Meyers, M. Kareev, X. Liu, Y. Cao, J. W. Freeland, and J. Chakhalian, *Phys. Rev. B* **98**, 045115 (2018).
- ⁵¹ S.-S. Lee, *Annual Review of Condensed Matter Physics* **9**, 227 (2018), <https://doi.org/10.1146/annurev-conmatphys-031016-025531>.
- ⁵² Supplemental Information.
- ⁵³ E. C. Jones, D. K. Christen, J. R. Thompson, R. Feenstra, S. Zhu, D. H. Lowndes, J. M. Phillips, M. P. Siegal, and J. D. Budai, *Phys. Rev. B* **47**, 8986 (1993).
- ⁵⁴ A. J. Hauser, E. Mikheev, N. E. Moreno, T. A. Cain, J. Hwang, J. Y. Zhang, and S. Stemmer, *Applied Physics Letters* **103**, 182105 (2013).
- ⁵⁵ G. Kresse and J. Furthmüller, *Computational Materials Science* **6**, 15 (1996).
- ⁵⁶ G. Kresse and J. Furthmüller, *Phys. Rev. B* **54**, 11169 (1996).
- ⁵⁷ J. P. Perdew, K. Burke, and M. Ernzerhof, *Physical Review Letters* **77**, 3865 (1996).
- ⁵⁸ P. E. Blöchl, *Physical Review B* **50**, 17953 (1994).
- ⁵⁹ G. Kresse and D. Joubert, *Physical Review B* **59**, 1758 (1999).
- ⁶⁰ R. S. Dhaka, T. Das, N. C. Plumb, Z. Ristic, W. Kong, C. E. Matt, N. Xu, K. Dolui, E. Razzoli, M. Medarde, L. Patthey, M. Shi, M. Radović, and J. Mesot, *Phys. Rev. B* **92**, 035127 (2015).
- ⁶¹ T. Das, J.-X. Zhu, and M. J. Graf, *Phys. Rev. Lett.* **108**, 017001 (2012).
- ⁶² T. Das and K. Dolui, *Phys. Rev. B* **91**, 094510 (2015).
- ⁶³ T. Das, R. Markiewicz, and A. Bansil, *Advances in Physics* **63**, 151 (2014), <https://doi.org/10.1080/00018732.2014.940227>.
- ⁶⁴ J.-S. Zhou, J. B. Goodenough, and B. Dabrowski, *Phys. Rev. Lett.* **94**, 226602 (2005).
- ⁶⁵ J. Ruppen, J. Teyssier, O. E. Peil, S. Catalano, M. Gibert, J. Mravlje, J.-M. Triscone, A. Georges, and D. van der Marel, *Phys. Rev. B* **92**, 155145 (2015).
- ⁶⁶ E. F. Schwier, R. Scherwitzl, Z. Vydrova, M. Garca-Fernandez, M. Gibert, P. Zubko, M. G. Garnier, J.-M. Triscone, and P. Aebi, *Phys. Rev. B* **86**, 195147 (2012).
- ⁶⁷ A. Damaselli, Z. Hussain, and Z.-X. Shen, *Rev. Mod. Phys.* **75**, 473 (2003).
- ⁶⁸ J. S. Lee, S. J. Moon, B. J. Yang, J. Yu, U. Schade, Y. Yoshida, S.-I. Ikeda, and T. W. Noh, *Phys. Rev. Lett.* **98**, 097403 (2007).
- ⁶⁹ T. Shimojima, T. Sonobe, W. Malaeb, K. Shinada, A. Chainani, S. Shin, T. Yoshida, S. Ideta, A. Fujimori, H. Kumigashira, K. Ono, Y. Nakashima, H. Anzai, M. Arita, A. Ino, H. Namatame, M. Taniguchi, M. Nakajima, S. Uchida, Y. Tomioka,

- T. Ito, K. Kihou, C. H. Lee, A. Iyo, H. Eisaki, K. Ohgushi, S. Kasahara, T. Terashima, H. Ikeda, T. Shibauchi, Y. Matsuda, and K. Ishizaka, *Phys. Rev. B* **89**, 045101 (2014).
- ⁷⁰ S. J. Allen, A. J. Hauser, E. Mikheev, J. Y. Zhang, N. E. Moreno, J. Son, D. G. Ouellette, J. Kally, A. Kozhanov, L. Balents, and S. Stemmer, *APL Materials* **3**, 062503 (2015).
- ⁷¹ S. D. Ha, R. Jaramillo, D. M. Silevitch, F. Schoofs, K. Kerman, J. D. Baniecki, and S. Ramanathan, *Phys. Rev. B* **87**, 125150 (2013).
- ⁷² J. Son, P. Moetakef, J. M. LeBeau, D. Ouellette, L. Balents, S. J. Allen, and S. Stemmer, *Applied Physics Letters* **96**, 062114 (2010).
- ⁷³ R. Eguchi, A. Chainani, M. Taguchi, M. Matsunami, Y. Ishida, K. Horiba, Y. Senba, H. Ohashi, and S. Shin, *Phys. Rev. B* **79**, 115122 (2009).
- ⁷⁴ H. K. Yoo, S. I. Hyun, L. Moreschini, H.-D. Kim, Y. J. Chang, C. H. Sohn, D. W. Jeong, S. Sinn, Y. S. Kim, A. Bostwick, E. Rotenberg, J. H. Shim, and T. W. Noh, *Sci. Rep.* **5**, 8746 (2015).
- ⁷⁵ J. Ruppen, J. Teyssier, I. Ardizzone, O. E. Peil, S. Catalano, M. Gibert, J.-M. Triscone, A. Georges, and D. van der Marel, *Phys. Rev. B* **96**, 045120 (2017).
- ⁷⁶ P. Gegenwart, Q. Si, and F. Steglich, *Nature Physics* **4**, 186 (2008).
- ⁷⁷ N. Doiron-Leyraud, P. Auban-Senzier, S. René de Cotret, C. Bourbonnais, D. Jérôme, K. Bechgaard, and L. Taillefer, *Phys. Rev. B* **80**, 214531 (2009).
- ⁷⁸ L. Taillefer, *Annual Review of Condensed Matter Physics* **1**, 51 (2010).
- ⁷⁹ G. R. Stewart, *Rev. Mod. Phys.* **83**, 1589 (2011).
- ⁸⁰ B. Keimer, S. A. Kivelson, M. R. Norman, S. Uchida, and J. Zaanen, *Nature* **518**, 179 (2015).
- ⁸¹ S. Banerjee, C. Dasgupta, S. Mukerjee, T. Ramakrishnan, and K. Sarkar, ArXiv e-prints (2018), [arXiv:1806.03854](https://arxiv.org/abs/1806.03854) [cond-mat.str-el].
- ⁸² T. R. Chien, Z. Z. Wang, and N. P. Ong, *Phys. Rev. Lett.* **67**, 2088 (1991).
- ⁸³ K. Rajeev, G. Shivashankar, and A. Raychaudhuri, *Solid State Communications* **79**, 591 (1991).
- ⁸⁴ P. W. Anderson, *Phys. Rev. Lett.* **67**, 2092 (1991).
- ⁸⁵ J. M. Harris, H. Wu, N. P. Ong, R. L. Meng, and C. W. Chu, *Phys. Rev. B* **50**, 3246 (1994).
- ⁸⁶ Y. Li, W. Tabis, G. Yu, N. Barišić, and M. Greven, *Phys. Rev. Lett.* **117**, 197001 (2016).
- ⁸⁷ S. Stemmer and S. J. Allen, *Reports on Progress in Physics* **81**, 062502 (2018).
- ⁸⁸ M. Uchida, Y. Yamasaki, Y. Kaneko, K. Ishizaka, J. Okamoto, H. Nakao, Y. Murakami, and Y. Tokura, *Phys. Rev. B* **86**, 165126 (2012).
- ⁸⁹ Y. Onose, Y. Taguchi, K. Ishizaka, and Y. Tokura, *Physical review letters* **87**, 217001 (2001).
- ⁹⁰ S. Badoux, W. Tabis, F. Laliberté, G. Grissonnanche, B. Vignolle, D. Vignolles, J. Béard, D. Bonn, W. Hardy, R. Liang, *et al.*, *Nature* **531**, 210 (2016).
- ⁹¹ R. Boyack, X. Wang, Q. Chen, and K. Levin, *Physical Review B* **99**, 134504 (2019).
- ⁹² Y. Dagan and R. Greene, *Physical Review B* **76**, 024506 (2007).
- ⁹³ Y. Dagan, M. Qazilbash, C. Hill, V. Kulkarni, and R. Greene, *Physical review letters* **92**, 167001 (2004).
- ⁹⁴ T. Das, R. Markiewicz, and A. Bansil, *Journal of Physics and Chemistry of Solids* **69**, 2963 (2008).